# Nonadiabatic excited-state molecular dynamics: Treatment of electronic decoherence

Tammie Nelson, Sebastian Fernandez-Alberti, Adrian E. Roitberg, and Sergei Tretiak

## Additional information on J. Chem. Phys.

# Nonadiabatic excited-state molecular dynamics: Treatment of electronic decoherence

Tammie Nelson,[1] Sebastian Fernandez-Alberti,[2] Adrian E. Roitberg,[3] and Sergei Tretiak[1]

[1]*Theoretical Division, Center for Nonlinear Studies (CNLS), and Center for Integrated Nanotechnologies (CINT), Los Alamos National Laboratory, Los Alamos, New Mexico 87545, USA*
[2]*Universidad Nacional de Quilmes, Roque Saenz Pea 352, B1876BXD Bernal, Argentina*
[3]*Departments of Physics and Chemistry, Quantum Theory Project, University of Florida, Gainesville, Florida 32611, USA*

Within the fewest switches surface hopping (FSSH) formulation, a swarm of independent trajectories is propagated and the equations of motion for the quantum coefficients are evolved coherently along each independent nuclear trajectory. That is, the phase factors, or quantum amplitudes, are retained. At a region of strong coupling, a trajectory can branch into multiple wavepackets. Directly following a hop, the two wavepackets remain in a region of nonadiabatic coupling and continue exchanging population. After these wavepackets have sufficiently separated in phase space, they should begin to evolve independently from one another, the process known as decoherence. Decoherence is not accounted for in the standard surface hopping algorithm and leads to internal inconsistency. FSSH is designed to ensure that at any time, the fraction of classical trajectories evolving on each quantum state is equal to the average quantum probability for that state. However, in many systems this internal consistency requirement is violated. Treating decoherence is an inherent problem that can be addressed by implementing some form of decoherence correction to the standard FSSH algorithm. In this study, we have implemented two forms of the instantaneous decoherence procedure where coefficients are reinitialized following hops. We also test the energy-based decoherence correction (EDC) scheme proposed by Granucci *et al.* and a related version where the form of the decoherence time is taken from Truhlar's Coherent Switching with Decay of Mixing method. The sensitivity of the EDC results to changes in parameters is also evaluated. The application of these computationally inexpensive *ad hoc* methods is demonstrated in the simulation of nonradiative relaxation in two conjugated oligomer systems, specifically poly-phenylene vinylene and poly-phenylene ethynylene. We find that methods that have been used successfully for treating small systems do not necessarily translate to large polyatomic systems and their success depends on the particular system under study. © 2013 AIP Publishing LLC. [http://dx.doi.org/10.1063/1.4809568]

## I. INTRODUCTION

Molecular dynamics with quantum transitions (MDQT) is a well tested, computationally efficient, conceptually simple, and accurate method for the simulation of nonadiabatic processes in which the nuclear and electronic systems are treated separately. Coupling the systems proves to be a non-trivial task. In the fewest switches surface hopping (FSSH) scheme, described by Tully,[1,2] the nuclei are treated classically while the electrons are treated within the quantum mechanical framework, and transitions between multiple coupled excited states are allowed depending on the strength of the nonadiabatic coupling. At any given time, the nuclei are evolved according to forces governed by the potential energy surface (PES) of a single adiabatic electronic excited state, the "current state." Meanwhile, the electron density evolves according to the value of the nonadiabatic couplings and nuclear velocities, where the velocities depend on the accelerations dictated by the current state.[3] In recent years, we have developed a nonadiabatic excited-state molecular dynamics (NA-ESMD) framework[3] capable of extending the FSSH formalism to large polyatomic molecules with many coupled electronic states. Recently, we have investigated the dependence of simulation results on convergence and parameters[4] and the success of NA-ESMD in modeling photoinduced dynamics including nonradiative relaxation and energy transfer has been demonstrated for a variety of large polyatomic systems.[5–10] In this paper, we continue to develop our NA-ESMD methodology by analyzing the affect of various *ad hoc* decoherence corrections.

MDQT is based on the independent trajectory approximation, that is, there is no interchange of information among trajectories. Within the FSSH formulation, the equations of motion for the quantum coefficients are propagated coherently along each nuclear trajectory. That is, the phase factors, or quantum amplitudes, are retained. At a region of strong coupling, a wavepacket can branch into multiple subpackets on each surface. Directly following a hop, the two subpackets remain in a region of nonadiabatic coupling and, following the FSSH prescription, they continue to undergo coherent time evolution. However, these subpackets should begin to evolve independently from one another after they have sufficiently separated in phase space, the process known as electronic decoherence.

**138**, 224111-1

Electronic decoherence is not accounted for in the standard Tully algorithm:[1,2] The interference between the quantum amplitudes of branching subpackets is neglected, causing the states to be more coherent than they should be. In principle, decoherence can be included by running a swarm of trajectories with the same initial conditions but with a different random number sequence used to determine hops between adiabatic states. Hops will occur at different times and the trajectories will differentiate from one another. When averaged together, the interference between the trajectoires provides the quantum decoherence. However, this must be done for an ensemble of different initial states requiring a double summation which dramatically increases the computational cost. Furthermore, if one of the divergent wavepackets passes through a region of strong coupling multiple times, the wavepacket may undergo yet another branching event, compounding the original decoherence problem.

Properly accounting for decoherence is an important effect which, in many cases, will influence the accuracy of the simulated results. It is important to note that decoherence can only be properly incorporated through a full density matrix formulation.[11] The FSSH formulation is designed to ensure that at any time, the fraction of classical trajectories evolving on each quantum state is equal to the average quantum probability for that state. However, in many systems this so-called "internal consistency" requirement is violated.[12,13] In general, the disagreement can be caused by classically forbidden transitions or by the divergence of independent trajectories following passage through a region of strong coupling. Classically forbidden transitions are the result of insufficient energy in the nuclear coordinates (in the direction of the nonadiabatic coupling) to conserve the total energy. Some improvements to the basic MDQT procedure have been proposed to eliminate classically forbidden transitions.[13,14] Diverging trajectories pose an inherent problem that can be addressed by implementing some form of decoherence correction to the standard Tully algorithm.[13,15–17]

A variety of methods to account for divergent trajectories by eliminating the coherence of the quantum amplitudes have been proposed.[12,13,16,18–25] One of the simplest methods of promoting internal consistency is resetting the quantum amplitude of the current state to unity after a classical trajectory passes through a nonadiabatic coupling region, thus removing the coherence of the quantum coefficients. This method is physically justified: at an avoided crossing a wavepacket will generally branch into two subpackets carrying the electronic populations. The subpackets, traveling on different surfaces, will separate in phase space and, since they are unlikely to interact again, the time average of their phase differences should be zero.

Different criteria for identifying coupling regions have previously been applied. For example, the quantum amplitudes can be reset when the magnitude of the nonadiabatic coupling vector between two adiabatic states becomes smaller than some specified tolerance after a maximum in the value of the nonadiabatic coupling has been reached.[13] Alternatively, a decoherence time can be explicitly included and can be estimated from the pure-dephasing time given by optical response or Redfield theory.[11] For times shorter than the decoherence time, the interference between the wavefunctions is maintained by coherent evolution. After the decoherence time, the trajectories diverge and the interference is eliminated by resetting the quantum amplitudes. However, implementation of this approach is often impractical for large systems involving many coupled electronic states since the decoherence time varies between each pair of states and is time dependent.[11,26] Despite this, the method has been applied quite successfully in simulations involving only two states.[27,28] Alternatively, in the presence of a strong external field, the electronic populations are re-initialized at the peaks of the field since most hops occur near the nodes of the laser cycle.[25] Here, we use hops to identify regions of coupling. Indeed, the classical trajectory is most likely to hop in a region of strong coupling. Therefore, coefficients are reset following hopping events and the coefficient of the current state following a hop is assigned a value of unity. We refer to this scheme as instantaneous decoherence (ID) since it is based on the assumption that following a hop, divergent wavepackets will instantaneously separate in phase space and should immediately undergo independent evolution.

Another method that has demonstrated its success in treating decoherence[29–31] while introducing little additional computational effort is the energy-based decoherence correction (EDC) developed by Granucci *et al.*[17,18] in which the coefficients are rescaled at each classical time step. The size of the scaling factor differs for each adiabatic state and is governed by the energy gap separating the state in question from the current running state. The correction is designed to equate the average quantum probability to the classical distribution of trajectories in each electronic state thereby eliminating coherence effects and restoring internal consistency. The EDC method is based on the decoherence time, $\tau_{\beta\alpha}$, proposed by the Truhlar group[24,32] and used in the Coherent Switching with Decay of Mixing method (CSDM). The CSDM decoherence time and the parameters involved in the expression have been applied to EDC with only a minor alteration to its functional form. Therefore, it is important to evaluate the role of parameters entering $\tau_{\beta\alpha}$ when applied to EDC schemes. It has previously been reported that "results are not very sensitive to the particular form of $\tau_{\beta\alpha}$ or to the values of the parameters, provided only that $\tau_{\beta\alpha}$ is large enough."[24] Further, the insensitivity of the CSDM results to changes in parameters was demonstrated for a three-dimensional atom-molecule system with two electronic states.[24] For large polyatomic systems, it is less clear whether the simulation results are independent of changes to the involved parameters.

In this study, we have implemented various practical heuristic decoherence schemes in order to determine the effects of decoherence on the simulated photoinduced dynamics in oligomer systems of poly-phenylene vinylene (PPV) and poly-phenylene ethynylene (PPE). Here we focus on the ID approach and the Granucci EDC algorithm (*G-EDC*). G-EDC is compared to a modified version of the algorithm in which the decoherence time has been replaced by the functional form originally proposed by Truhlar (*T-EDC*). We also demonstrate an alternative ID procedure in which coefficients are reinitialized not only after successful hops, but at all attempted hops as well, regardless of whether the hop is allowed

or forbidden. We have compared these methods to the standard Tully surface hopping routine. We have also evaluated the sensitivity of the G-EDC result to changes in the parameters involved in calculating the decoherence time.

In Sec. II, we will briefly describe our nonadiabatic excited-state molecular dynamics (NA-ESMD) approach and simulation details, and a description of the decoherence algorithms is also provided. Internal consistency is discussed and the physical quantities that serve as indicators are defined. Finally, we present the results for the simulated photoinduced dynamics of both PPV and PPE systems paying close attention to the choice of parameters used for G-EDC. The evolution of the state populations, quantum wavepackets, and quantum coefficients are analyzed to determine the effect of decoherence on the simulated dynamics.

## II. THEORETICAL METHODOLOGY

The NA-ESMD model combines the FSSH algorithm, as it is used in the MDQT method,[1,33] with "on the fly" calculation of the electronic energies, gradients, and nonadiabatic coupling vectors for the excited states using a Collective Electronic Oscillator (CEO) package.[34–37] The CEO code is based on well-tested semiempirical models combined with the Time-Dependent Hartree-Fock (TDHF) or the Configuration Interaction singles (CIS) formalism to describe correlated excited states. A detailed description of the CEO code and NA-ESMD implementation can be found in Refs. 3, 34, 38, and 39.

### A. Standard Tully surface hopping

According to the standard Tully FSSH procedure,[1] for each trajectory, the forces acting on the classical subsystem are determined by a single adiabatic state, the current state $\alpha$. Meanwhile, the total electronic wavefunction is a mixed state, expanded in terms of the adiabatic basis functions, $\phi_i(\mathbf{r}; \mathbf{R}(t))$,

$$\Psi(x, R, t) = \sum_i c_i(t)\phi_i(\mathbf{r}; \mathbf{R}(t)), \tag{1}$$

where $c_i(t)$ are the time-dependent expansion coefficients, and $\mathbf{r}$ represents the electronic degrees of freedom. The equation of motion for the coefficients can be obtained by substituting Eq. (1) into the time-dependent Schrödinger equation resulting in the following expression:

$$i\hbar \frac{\partial c_i(t)}{\partial t} = c_i(t)E_i - i\hbar \sum_j c_j(t)\dot{\mathbf{R}} \cdot \mathbf{d}_{ij}, \tag{2}$$

where the nonadiabatic coupling vector is defined as $\mathbf{d}_{ij} = \langle \phi_i(R)|\nabla_R \phi_j(R) \rangle$ and the corresponding scalar value is given by $\dot{\mathbf{R}} \cdot \mathbf{d}_{ij} = \langle \phi_i | \frac{\partial \phi_j}{\partial t} \rangle$. The diagonal elements of the time-dependent density matrix with elements $a_{ij}(t) = c_i^*(t)c_j(t)$ give the occupation probabilities of the adiabatic states. The probability that the nuclear trajectory will hop from the current electronic state $\alpha$ to some other state $\beta$ during the time interval $\Delta t$ is given by

$$g_{\alpha\beta} = \Delta t \frac{b_{\beta\alpha}(t)}{a_{\alpha\alpha}(t)}, \tag{3}$$
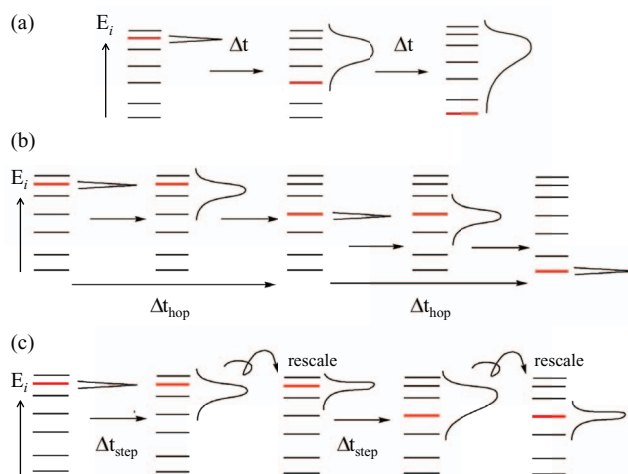


FIG. 1. Cartoon depicting the evolution of the quantum amplitudes $c_i$ during nonradiative relaxation. The wavefunction is initialized as a pure state. The red state symbolizes the "current state." (a) During the standard Tully procedure, the wavepacket continues to broaden but remains at relatively high energy even as the system transitions to lower energy states. (b) Following instantaneous decoherence the wavepacket is allowed to broaden, but the coefficients are reinitialized after each hop so that the new current state has a probability of unity. In this way, the wavepacket center follows the relaxation to lower energy. (c) In energy-based decoherence, the wavepacket broadens slightly after each timestep and the coefficients are rescaled to narrow the wavepacket before the next timestep. The damping factor is related to the energy separation from the current state. Population removed from other states is deposited into the current state so that the center of the wavepacket follows the relaxation to lower energy.

where $b_{\beta\alpha}(t) = -2Re(a_{\alpha\beta}^*\dot{\mathbf{R}} \cdot \mathbf{d}_{\alpha\beta})$ is related to the probability flux.

Figure 1(a) demonstrates the internal inconsistency which results from the decoherence problem in the standard Tully FSSH formulation. The electronic wavefunction is initialized as a pure state. The coefficients are allowed to evolve according to Eq. (2) and after some time $\Delta t$ the wavepacket has broadened as some of the quantum amplitude is transferred to lower energy states and the classical system undergoes hopping. As the classical system continues to relax to lower energy, the quantum wavepacket gets "left behind." That is, the wavepacket remains centered at higher energy with respect to the current state with only a small quantum probability for the lowest energy state despite that it is the classically occupied state.

In Secs. II B and II C, we will introduce practical heuristic methods developed to include decoherence in a phenomenological way.

### B. Instantaneous decoherence

The evolution of the wavepacket using ID is illustrated schematically in Fig. 1(b). Following the ID procedure, the electronic wavefunction is again initialized as a pure state, and coefficients are allowed to evolve according to Eq. (2). The wavepacket broadens and some of the population is transferred to lower energy states allowing the classical system to hop. However, after each successful hop, the quantum coefficients are reinitialized and a coefficient of one is assigned to the new current state, while the populations for all other

states are erased. This routine is based on the assumption that divergent wavepackets will instantly separate in phase space and should immediately undergo independent evolution. After resetting the coefficients, the standard coefficient evolution once again takes over and the wavepacket again broadens until another hopping event occurs at which point the process of resetting the coefficients will be repeated. Thus, the wavepacket undergoes a series of broadening and collapsing events mediated by the hopping frequency. In this way, after each hop, the center of the wavepacket is realigned with the current state and internal consistency is improved.

We call the above procedure *ID-S*, since the coefficients are reinitialized only after successful hops. One can imagine that all attempted hops should also be treated as decoherence events, regardless of whether the hop is allowed or forbidden due to energy constraints. We call the method of resetting the coefficients after every attempted hop *ID-A*. If the hop is accepted, the wavepacket is collapsed to the new state using the same procedure for ID-S. In addition, if the hop is forbidden, the wavepacket is collapsed back to the current running state. For example, suppose a hop from $S_1 \rightarrow S_2$ is predicted. If the hop is successful, the coefficient of $S_2$ will be set to one and the system will begin evolving on $S_2$. If the hop is forbidden, the coefficient of $S_1$ will be set to one and the system will continue evolving on $S_1$.

## C. Energy-based decoherence correction

The energy-based decoherence correction relies on rescaling the quantum coefficients after each classical timestep, as illustrated schematically in Fig. 1(c). The electronic wavefunction is again initialized as a pure state, and coefficient evolution is governed by Eq. (2). However, the wavepacket is not permitted to undergo the natural broadening. After each nuclear timestep, the coefficients are rescaled (damped) and the wavepacket is narrowed before continuing the evolution using the rescaled values.

In the G-EDC[17,18] formulation, rescaling is performed according to the following procedure for all states $\beta \neq \alpha$ where $\alpha$ denotes the current state

$$c'_\beta(t) = c_\beta(t)e^{-\Delta t/\tau_{\beta\alpha}(t)}. \tag{4}$$

Here $c_\beta(t)$ is the original expansion coefficient and $c'_\beta(t)$ is the damped coefficient that is used to continue the evolution for the subsequent timestep. The decoherence time, $\tau_{\beta\alpha}(t)$, is given by

$$\tau_{\beta\alpha}(t) = \frac{\hbar}{|E_\beta(t) - E_\alpha(t)|}\left(C + \frac{E_0}{E_{kin}(t)}\right), \tag{5}$$

whose value is inversely proportional to the energy separation between the current state $\alpha$ and some other state $\beta$ given by $|E_\beta(t) - E_\alpha(t)|$. C is a unitless parameter greater than or equal to one, $E_0$ is a positive parameter with units of energy, and $E_{kin}(t)$ is the *total* kinetic energy. In order to preserve detailed balance and ensure that the center of the wavepacket follows the current state, the population removed from all $\beta \neq \alpha$ states

is deposited into the current state $\alpha$,

$$c'_\alpha(t) = c_\alpha(t)\left[\frac{1 - \sum_{\beta \neq \alpha}|c'_\beta t|^2}{|c_\alpha(t)|^2}\right]^{1/2}. \tag{6}$$

The decoherence time $\tau_{\beta\alpha}(t)$ used above is a simplification of the decoherence time introduced by Truhlar and co-workers in the CSDM method.[24,32] The full expression for the decoherence time is given by

$$\tau_{\beta\alpha}(t) = \frac{\hbar}{|E_\beta(t) - E_\alpha(t)|}\left(C + \frac{E_0}{(\mathbf{P} \cdot \hat{s})^2/2\mu}\right), \tag{7}$$

where $\mathbf{P}$ is the momentum and $\hat{s}$ is electron-nuclear coupling vector. The term in the denominator of $E_0$ can be interpreted as the *projection* of the kinetic energy in the direction of the nonadiabatic coupling vector. In G-EDC, this term is assumed to be equivalent to the total kinetic energy for simplicity. The expression used in G-EDC (Eq. (5)) is less computationally demanding since it does not require the nonadiabatic coupling vector to be evaluated at each nuclear timestep; In the standard FSSH method, this term is usually evaluated only after a hop when it is used for velocity rescaling.[40] For T-EDC, we have simply replaced the decoherence time from Eq. (5) used in G-EDC with the original decoherence time given by Eq. (7). The values of the parameters C and $E_0$ are of considerable interest here. C is a unitless parameter taken to be one, and $E_0$ is assigned a value of 0.1 hartree in agreement with previous studies.[17,18,24,32]

## D. Internal consistency

Internal inconsistency in FSSH simulations is manifested as a discrepancy between the classical and quantum subsystems. To check for internal consistency in our systems we analyze the state populations. The population can be defined within the nuclear (classical) or electronic (quantum) picture. It is well known that in FSSH simulations, the state populations can be expressed as the fraction of trajectories evolving on the state of interest at any given time or as the quantum probability for the state averaged over the ensemble of trajectories. The former is a classical representation, while the latter provides a quantum description.

The classical population for some state $i$ can be written as

$$P_i^C(t) = N_i(t)/N_{traj}, \tag{8}$$

where $N_i(t)$ is the number of trajectories evolving on the $i$th state at any given time and $N_{traj}$ is the total number of trajectories in the ensemble. The familiar quantum populations are given by the quantum probability for the state of interest averaged over the ensemble of trajectories

$$P_i^Q(t) = \langle|c_i(t)|^2\rangle_{N_{traj}}, \tag{9}$$

where $c_i(t)$ is the appropriate expansion coefficient for the $i$th electronic state.
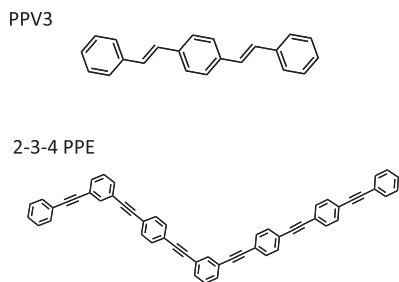
PPV3

2-3-4 PPE

FIG. 2. The model molecular systems studied with the NA-ESMD approach: A 3-ring oligomer of PPV (PPV3), and a system composed of meta-substituted linear PPE segments of 2-, 3-, and 4-rings (2-3-4 PPE).

## III. RESULTS AND DISCUSSION

In order to investigate decoherence effects, we have performed NA-ESMD simulations of the photoinduced dynamics of the two model systems depicted in Fig. 2: A 3-ring oligomer of PPV (PPV3), and a system composed of meta-substituted linear PPE segments of 2-, 3-, and 4-rings (2-3-4 PPE). We implemented both the ID-S and ID-A procedures in which the quantum coefficients are reinitialized either after each successful hop (ID-S) or after each attempted hop (ID-A). Simulations were also performed using the G-EDC algorithm as well as the modified T-EDC algorithm using the full decoherence time. These decoherence schemes have been compared to the standard Tully FSSH algorithm with no decoherence correction.

### A. Molecular dynamics simulations

NA-ESMD simulations were performed on PPV3 and 2-3-4 PPE to model the nonradiative relaxation following photoexcitation to a high energy excited state at room temperature. For all simulations presented here, the AM1/CIS level of theory has been used.

We start our simulations by running Born-Oppenheimer (BO) molecular dynamics in the ground electronic state at room temperature for 600 ps using a timestep of $\Delta t = 0.5$ fs. The systems are heated and allowed to equilibrate to a final temperature of 300 K during the first 10 ps. The Langevin thermostat[41] was used to maintain constant temperature with a friction coefficient $\gamma = 2.0$ ps$^{-1}$. Following the equilibration period, snapshots were collected to provide the initial positions and momenta for the subsequent excited state simulations. Each configuration corresponds to an independent trajectory in NA-ESMD.

For the sampled configurations, excited state energies and oscillator strengths were calculated. The initial state was chosen according to a Frank-Condon window defined as

$$g_i(r, \mathbf{R}) = \exp[-T^2(E_{laser} - \Omega_i)^2], \quad (10)$$

where $E_{laser}$ represents the energy of a laser, and $\Omega_i$ represents the energy of the $i$th state (expressed in units of fs$^{-1}$) from the theoretical absorption spectrum. The laser shape is assumed to be Gaussian $f(t) = \exp(-t^2/2T^2)$, $T^2 = 42.5$ fs corresponding to a FWHM of 100 fs. The initial excitation is
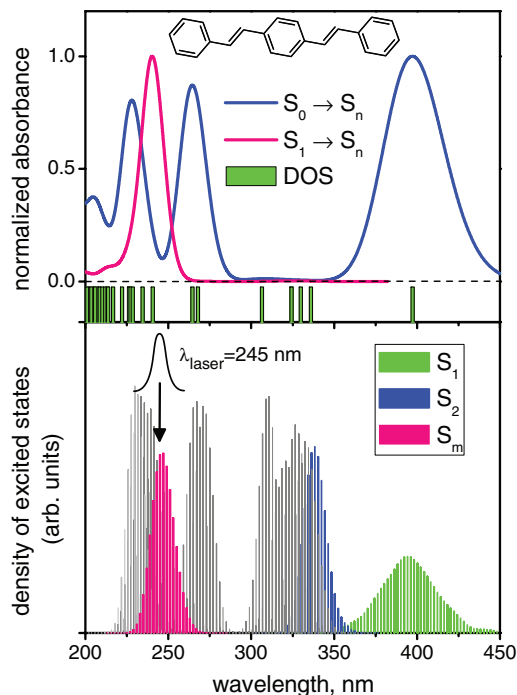
selected according to the relative values of $g_i(r, \mathbf{R})$ weighted by the oscillator strengths of each state.

The top panel in Fig. 3 displays the calculated normalized linear absorption spectrum ($S_0 \rightarrow S_n$) for PPV3 computed at the ground state AM1 optimized geometry as well as the equilibrium density of singlet excited states. The calculated nonlinear absorption from the lowest energy excited state ($S_1 \rightarrow S_n$) is also shown revealing a single strong absorbance feature which is not accessible from the ground state due to symmetry. This state is assigned as the $S_m$ state and it is the state with the highest oscillator strength from $S_1$. The $S_m$ excitation is one of the essential electronic states in conjugated polymers, which can be routinely observed using time-resolved pump-probe or electroabsorption spectroscopies.[42,43] Snapshots were collected from the ground-state MD at 500 fs intervals and all of the initial configurations were used to construct the density of excited states for the lowest 15 excited states shown in the bottom panel of Fig. 3 where the height of the spectrum corresponds to the number of configurations with a state at the given energy. Excitation to $S_m$ was performed according to Eq. (10) using a laser centered at $\lambda_{laser} = 245$ nm and the excited state energies and oscillator strengths from the theoretical $S_1 \rightarrow S_n$ absorption spectrum. We found that for the $S_m$ state, $m$ varied from 8 to 12 due to conformational disorder. A swarm of 540 excited-state trajectories was propagated at T = 300 K for 1 ps, where 15 electronic excited states have been included in the simulations. A classical time step $\Delta t = 0.1$ fs with $N_q = 3$ quantum steps between each classical step was used.



FIG. 3. (Top) Equilibrium absorption spectrum for PPV3 showing absorbance from the ground state ($S_0 \rightarrow S_n$), the lowest excited state ($S_1 \rightarrow S_n$) and equilibrium density of states. (Bottom) Density of excited states for the lowest 15 excited states at T = 300 K computed using all initial ground state configurations. $S_m$ is the state with the largest oscillator strength from $S_1$, and the excitation is performed using a simulated laser pulse centered at $\lambda = 245$ nm with FWHM = 100 fs.
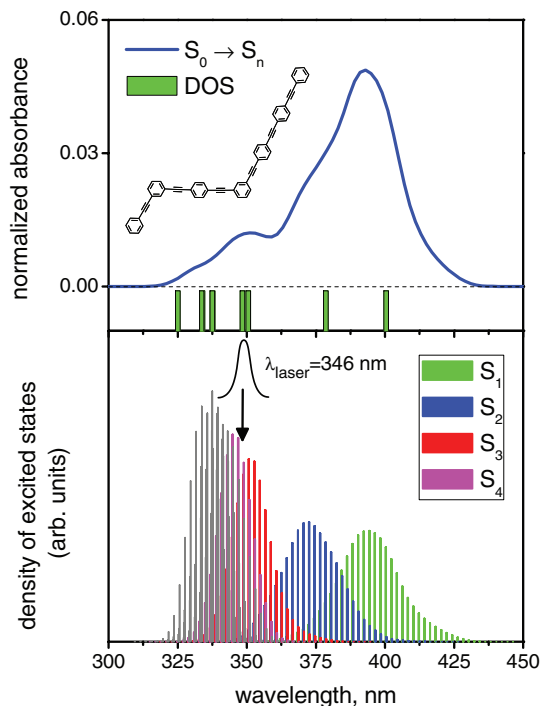
FIG. 4. (Top) Equilibrium absorption spectrum for 2-3-4 PPE showing absorbance from the ground state ($S_0 \rightarrow S_n$) and equilibrium density of states. (Bottom) Density of excited states for the lowest 6 excited states at T = 300 K computed using all initial ground state configurations. The excitation is performed using a simulated laser pulse centered at $\lambda$ = 346 nm with FWHM = 100 fs.

For the 2-3-4 PPE system, the normalized linear absorption spectrum for the AM1 optimized geometry and equilibrium density of states is shown in the top panel of Fig. 4. Snapshots were collected from the ground-state MD at 1 ps intervals and used to construct the density of excited states spectrum for the lowest 6 excited states in the bottom panel of Fig. 4 where the contribution of each state is shown. Excitation to the highly excited $S_n$ state localized on the 2-ring segment was performed according to Eq. (10) using a laser centered at $\lambda_{laser}$ = 346 nm where the energies and oscillator strengths for the lowest 10 excited states have been considered. Because of the strong overlap between the absorbance of individual states, $S_n$ corresponds to a range of states including $S_4$, $S_5$, $S_6$, and $S_7$. A swarm of 490 excited-state trajectories was propagated at T = 300 K for 200 fs where 10 electronic excited states have been included in the simulations. A classical time step $\Delta t$ = 0.2 fs with $N_q$ = 4 quantum steps between each classical step was used.

## B. Effective energy gaps

The two systems vary greatly in terms of the energy spacing between excited states, and coupling between states. From a general inspection of the density of states (DOS) and excited state spectra shown in Figs. 3 and 4, PPV3 contains larger gaps in its density of states, while the PPE system has only two relatively smaller gaps and has more pronounced overlap in the contributions to its spectrum. This is expected since our PPE system is composed of linear segments of
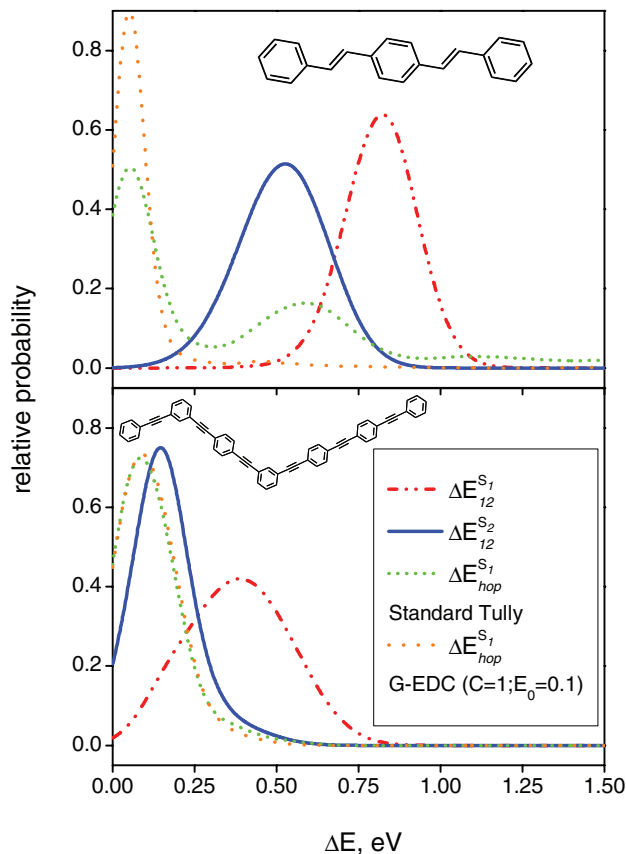


FIG. 5. Histograms of the energy gap between $S_1$ and $S_2$ are shown for PPV3 (top) and 2-3-4 PPE (bottom), while the system is evolving on $S_1$ ($\Delta E_{12}^{S_1}$) and $S_2$ ($\Delta E_{12}^{S_2}$) as well as the energy gap for the final effective hop to $S_1$ ($\Delta E_{hop}^{S_1}$) during Standard Tully dynamics and for G-EDC. Energy gaps are smaller in 2-3-4 PPE and the final effective hop corresponds to the most probably energy gap for $S_2$. In PPV3, energy gaps are large, and the final effective hop can only be made from lower energies, which are infrequent in the $S_2$ spectrum.

varying lengths allowing the total absorption spectrum to be interpreted as the sum of the contributions from each fragment with strong overlap between the component absorption spectra.[5,10]

During our dynamics, we investigate the energy gap between $S_1$ and $S_2$. Figure 5 displays histograms of the energy gap $\Delta E_{12}$ while nuclei are moving on $S_2$ ($\Delta E_{12}^{S_2}$) and $S_1$ ($\Delta E_{12}^{S_1}$), and the energy gap for the final effective hop to $S_1$ ($\Delta E_{hop}^{S_1}$). The average values of the energy gaps are provided in Table I. First, the gaps for 2-3-4 PPE are smaller

TABLE I. Energy gaps between states $S_1$ and $S_2$ for the AM1 optimized structures and averaged during dynamics while running on $S_1$, $S_2$, and the final effective hop to $S_1$.

|  | 2-3-4 PPE (eV) | PPV3 (eV) |
|---|---|---|
| $\Delta E_{12}^{o}$ | 0.18 | 0.57 |
| $\Delta E_{12}^{S_1}$ | 0.38 | 0.82 |
| $\Delta E_{12}^{S_2}$ | 0.15 | 0.52 |
| $\Delta E_{hop}^{S_1}$ (Tully) | 0.10 | 0.36 |
| $\Delta E_{hop}^{S_1}$ (G-EDC) | 0.09 | 0.11 |

than for PPV3 as expected based on the density of states for the optimized geometry ($\Delta E_{12}^o$). In both systems, we observe evidence of "shishiodoshi" type unidirectional transfer recently demonstrated by our group in phenylene ethynylene dendrimers[5] where the energy gap increases once the system transfers to the lower energy surface. That is, while the system is evolving on $S_2$, the energy gap between $S_2$ and $S_1$ remains small, and the energy flows between them. Once the electronic population has been substantially transferred to the lower energy state, the nuclear motion on the new surface decouples these states and the surfaces separate from each other such that $\Delta E_{12}^{S_2} < \Delta E_{12}^{S_1}$, thereby reducing successful transitions to higher energy.

Based on the relative energy gaps, we can expect relaxation to be faster in 2-3-4 PPE than in PPV3. Also, the energy gap associated with the final effective hop to $S_1$ indicates that for 2-3-4 PPE, the most probable hopping energy coincides very well with the most probable gap when the system is evolving on $S_2$, that is $\Delta E_{hop}^{S_1} \approx \Delta E_{12}^{S_2}$, so the gap does not impose any limitations on hopping. However, the situation is drastically different for PPV3. Here $\Delta E_{hop}^{S_1} < \Delta E_{12}^{S_2}$ meaning that hops occur at a much lower energy gap coinciding with values of $\Delta E_{12}^{S_2}$ that are relatively improbable. During Standard Tully dynamics, only a small portion of hops occur at the most probable $\Delta E_{12}^{S_2}$. In G-EDC dynamics, no hops occur at larger energy gaps. Indeed, it is very unlikely for the system to overcome the large energy gap between $S_1$ and $S_2$ and it can only do so when the surfaces move close together,

a rare event. Because $S_2$ acts as a bottleneck in the dynamics of PPV3, we use the combined state populations from $S_1$ and $S_2$ in our analyses.

## C. Relaxation rates and internal consistency

Figure 6 shows the combined population rise of the two lowest energy states ($S_1+S_2$) in the top panels, and the rise of the lowest energy $S_1$ state in the bottom panels for both PPV3 and 2-3-4 PPE. Populations for the classical system are depicted as solid lines, while the corresponding dashed lines give the quantum probabilities. The classical population represents the fraction of trajectories evolving on a given state (Eq. (8)) and the average quantum probability gives the quantum populations for that state (Eq. (9)).

Looking first at the rise of the classical populations, the rate of relaxation is slower for all decoherence methods compared to the Standard Tully algorithm, as expected. Decoherence corrections remove population from lower energy states, either by collapsing the quantum wavefunction to a pure state or by rescaling the quantum coefficients. Population buildup in lower energy states is a requirement for a nonzero hopping probability according to Eq. (3) where $g_{\alpha\beta}(t) \sim c_\beta(t)$. Resetting or reducing the coefficients restricts the population buildup and the transition probabilities are reduced, hence, relaxation becomes slower.[44] For G-EDC, we use the previously recommended[17,18,24,32] parameters ($C = 1$; $E_0 = 0.1$ hartree). For both systems, G-EDC results in much slower
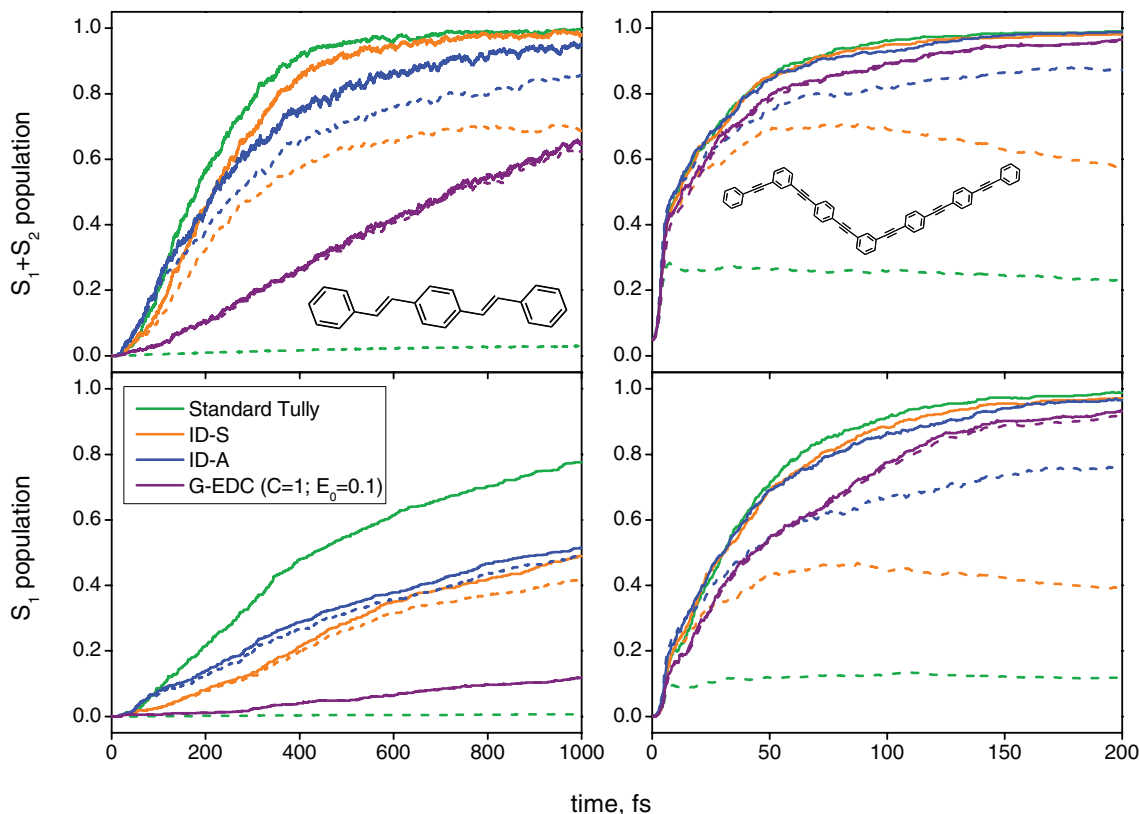


FIG. 6.  (Top) Combined population rise of the two lowest energy states ($S_1 + S_2$) and (bottom) population rise of the lowest energy $S_1$ state. Results are shown for ID-S, ID-A, and G-EDC using the recommended parameters ($C = 1$; $E_0 = 0.1$ hartree) compared to the Standard Tully algorithm. Populations for the classical system are depicted as solid lines while the corresponding dashed lines represent the average quantum probabilities.

dynamics compared to the other methods, and this difference is enhanced in PPV3. This can be understood by the fact that PPV3 has larger gaps in its density of states, that is, there are large energy gaps separating the current state from the states below so that coefficients of states below the large gap will experience a larger damping factor than in a system, such as 2-3-4 PPE, where the energy gaps are small. This can be seen from the form of $\tau_{\beta\alpha}$ in Eq. (5) where the decoherence time is inversely proportional to the energy separation. For large energy gaps, the decoherence time is smaller and the exponent in Eq. (4) becomes large leading to a smaller portion of the original population being maintained in the rescaled coefficients.

Comparing the population rise of $S_1 + S_2$ to $S_1$ alone, the large energy gap between $S_2$ and $S_1$ in PPV3 creates a bottleneck where population builds up in $S_2$ and is not able to transfer to $S_1$. Using Standard Tully, the coefficient evolution is not restricted and population is quickly transferred to $S_1$. Whereas for G-EDC, $S_1$ population comprises only a small fraction of the combined population as the system is restricted from overcoming the gap. However, in 2-3-4 PPE, there is no bottleneck; the majority of the combined population is in $S_1$, signifying that $S_2$ is a fast intermediate state and population is quickly transferred to $S_1$. This can also be seen in the energy gap histograms in Fig. 5 for the final effective hop to $S_1$ ($\Delta E_{hop}^{S_1}$). In PPV3, Standard Tully propagation produces a bimodal energy gap distribution with a small portion of hops to $S_1$ occurring at larger energy separations whereas in G-EDC, all of the hops occur at the lowest energy separation because the system cannot overcome the large $\Delta E_{12}^{S_2}$ energy gap. In PPE, the hopping energy is not affected by G-EDC because $\Delta E_{12}^{S_2}$ is small.

Next we consider internal inconsistency, which is apparent in the population curves. The growth of the average quantum probability is "lagging behind" their classical partners indicating that part of the quantum amplitude remains in higher energy states despite that the classical system has transitioned to lower energy. The most severe example is the Standard Tully algorithm, where the quantum probability remains very low indicating that the wavepacket is "trapped" in higher energy states throughout the dynamics, even after all of the trajectories have reached $S_1$ or $S_2$. All of the decoherence corrections offer some improvement in the internal consistency between the quantum and classical subsystems. For both systems, we find that G-EDC (using the recommended parameters) produces excellent agreement between the quantum and classical populations. This should not come as a surprise since G-EDC damps the coefficients of states other than the current state and deposits the remaining population into the current running state *at each timestep*. By continuously transferring population to the current state from all other states, internal consistency is maintained throughout the dynamics.

The ID-S procedure produces a peculiar effect, that is at short times internal consistency seems to be improved, while for long times the classical and quantum subsystems begin to diverge. This is especially pronounced in 2-3-4 PPE. For both of the ID algorithms, we expect some level of internal inconsistency simply due to the fact that hops are separated by some finite time interval, during which the coefficients undergo standard evolution. We first consider the results of ID-S, where there are two sources of internal inconsistency which lead to a problematic divergence of the quantum and classical subsystems. First, after the system has made the final effective hop, the coefficients will no longer be reset and they will undergo standard evolution causing the quantum and classical systems to diverge. Second, in systems with large energy gaps in the density of excited states, a similar (but less profound) divergence can also occur due to infrequent hops separated by long time intervals; in the intervals between hops, the coefficients will again evolve according to the Standard Tully procedure. We find that 2-3-4 PPE is largely affected by the former mechanism, while PPV3 shows the latter effect. In 2-3-4 PPE, there is a reasonably good agreement between the classical and quantum subsystems at short times. This good agreement at early times can be attributed to the small energy gaps (see the density of states in Fig. 4) and frequent hops. However, at later times the classical and quantum subsystems dramatically diverge; ultimately, the quantum probability even begins to decrease! Relaxation in 2-3-4 PPE is very fast and, in addition, it is unidirectional where the surfaces separate after the last effective hop making it virtually impossible to transition back to higher energy. The system quickly reaches $S_1$ and is then restricted from hopping. For the rest of the dynamics, the coefficients evolve according to Standard Tully resulting in divergence. In PPV3, relaxation is slow and states are separated by large energy gaps, thus leading to a prolonged period of hopping where each hop is well separated in time.

In order to overcome these deficiencies, we have implemented the ID-A algorithm where all attempted hops are treated as decoherence events regardless of whether the hop is allowed or forbidden. Again, we expect some level of internal inconsistency simply due to the fact that there is still some finite time interval between attempted hops. The results in Fig. 6 show a dramatic improvement in the internal consistency of ID-A compared to ID-S due to the increased frequency of wavepacket collapsing events which allow the quantum wavepacket to be periodically "realigned" with the current running state. The agreement between the classical and quantum systems is qualitatively much better, and the divergence at long times has been eliminated. In 2-3-4 PPE, there are numerous attempted hops from $S_1 \rightarrow S_2$ at the end of the dynamics that are forbidden due to insufficient kinetic energy to overcome the increased $S_2$-$S_1$ energy gap. Using the ID-A method, these hops have been accounted for. In PPV3, attempted hops throughout the relaxation effectively reduce the interval between hops, leading to improved agreement.

## D. Energy-based decoherence correction

In this section, we will take a closer look at how the form and value of the decoherence time, $\tau_{\beta\alpha}$, affects the internal consistency and the overall rate of relaxation in the G-EDC results. Figure 7 shows a comparison between G-EDC and T-EDC results using the recommended parameters (C = 1; $E_0$ = 0.1 hartree). For PPV3, the populations are shown for $S_1$, $S_2$, and the initial $S_m$ state. Populations for $S_1$, $S_2$, and $S_3$
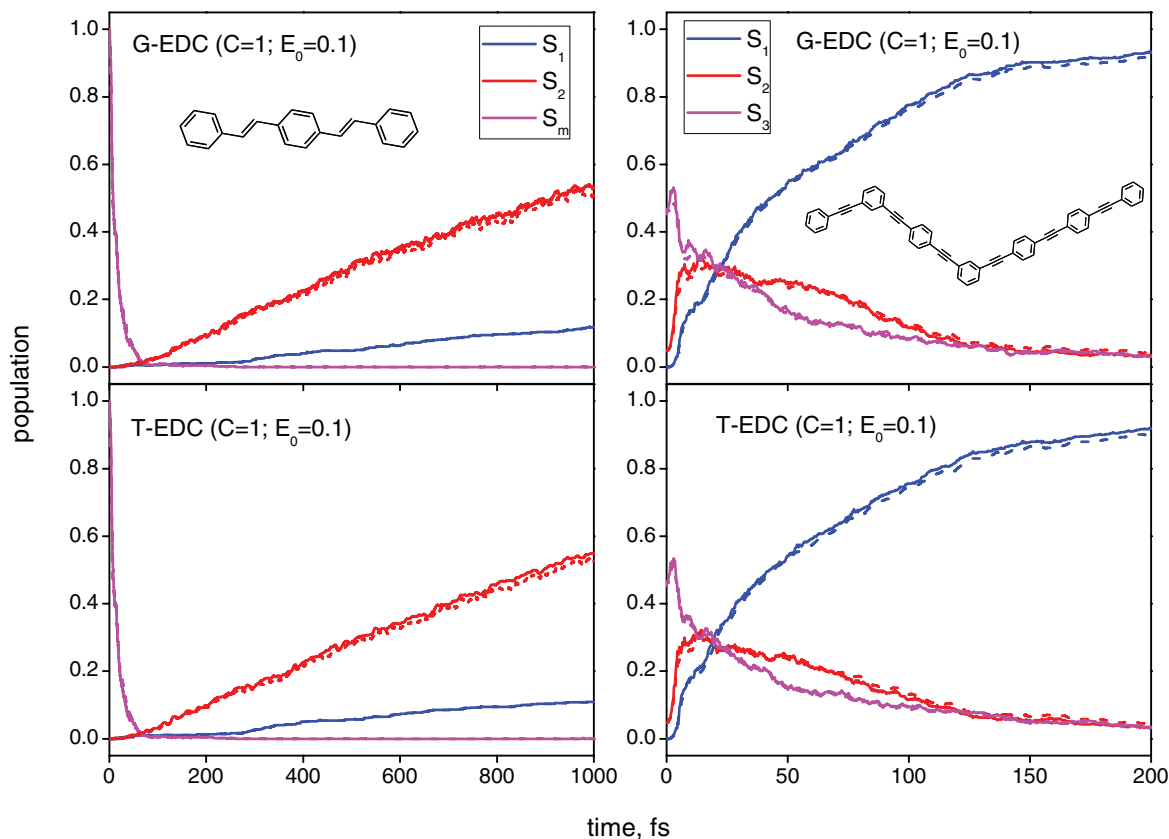
FIG. 7. Comparison of (top) G-EDC and (bottom) T-EDC populations using the recommended parameters (C = 1; $E_0$ = 0.1 hartree). For PPV3, the populations are shown for $S_1$, $S_2$, and the initial $S_m$ state. Populations for $S_1$, $S_2$, and $S_3$ are shown for 2-3-4 PPE. Classical populations and average quantum probabilities are depicted as solid and dashed lines, respectively.

are shown for 2-3-4 PPE. The classical populations and average quantum probabilities are depicted as solid and dashed lines, respectively. In both cases, we find that replacing the approximate form of $\tau_{\beta\alpha}$ used in the G-EDC implementation (Eq. (5)) with the full expression used in T-EDC (Eq. (7)) does not produce any change in either the rate or internal consistency of the simulated results. Therefore, we confirm that the kinetic energy in the direction of the nonadiabatic coupling vector can be approximated by the total kinetic energy for the systems studied in this work. This approximation allows us to avoid the computation of the nonadiabatic coupling vector at every timestep. However, for regions of phase space at which the states are not strongly coupled, it is expected that the nuclear motion in the direction of the nonadiabatic coupling vector is not particularly active, and this is more pronounced at low temperatures.

Let us consider the value of $\tau_{\beta\alpha}$. We can imagine that at each timestep of G-EDC, the wavepacket is being "squeezed," or narrowed, around the current state. The amount of "squeezing" is in proportion to the size of $\tau_{\beta\alpha}$. For small values of $\tau_{\beta\alpha}$, the damping term becomes large and the wavepacket will be very narrow. For larger values of $\tau_{\beta\alpha}$, coefficients experience less damping and the wavepacket is not squeezed as much. The narrowing of the wavepacket has two effects: first, it slows relaxation as population is removed from low energy states. Second, by adding population removed from other states to the current state, internal consistency is maintained.

The value of $\tau_{\beta\alpha}$, which determines the amount of damping, should have a huge effect on the overall dynamics. Intuitively, as the decoherence time approaches infinity, the damping effect will disappear and the Standard Tully result should be recovered.

We have already seen that for systems with large energy gaps, more population is removed from states with larger energy separation from the current state. Likewise, the value of $\tau_{\beta\alpha}$ can be increased or decreased by varying the parameters C and $E_0$. Figure 8 displays the population curves for relaxation in PPV3 and 2-3-4 PPE using G-EDC with various sets of parameters. Starting from the recommended parameters (C = 1; $E_0$ = 0.1 hartree), we simultaneously increased both C and $E_0$ up to (C = 10 000; $E_0$ = 1000 hartree) to represent "infinite" decoherence time. As usual, the classical population (fraction of trajectories) is represented by the solid lines, and the dashed lines represent the corresponding average quantum probabilities. As $\tau_{\beta\alpha}$ is increased, coefficients experience less damping and the overall relaxation rate increases as population buildup in lower energy states becomes less hindered. At the same time, internal consistency gets worse since not as much population is being redistributed into the current state, that is the wavepacket is not forced to be centered there.

The curves look very different for the two different systems. In 2-3-4 PPE, the classical population does not change very much with changes in parameters, the results seem relatively stable. In the case of PPV3, however, the dependence
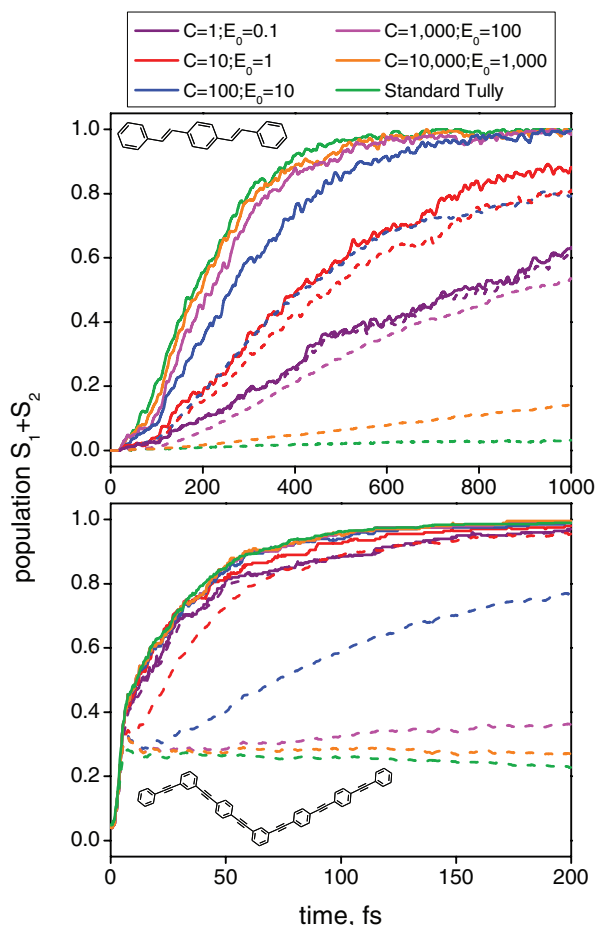
FIG. 8. Combined population rise for the lowest two excited states ($S_1 + S_2$) using G-EDC algorithm with varying parameters ($C$, $E_0$) for (top) PPV3 and (bottom) 2-3-4 PPE. Classical populations are shown as solid lines and the corresponding dashed lines represent the average quantum probabilities.

of the results on the value of $\tau_{\beta\alpha}$ is significant, and there is no stable region until we reach the largest (infinite) decoherence times. Meanwhile, the internal consistency shows less agreement as the parameters are increased for both systems, as expected. Again, PPV3 shows a greater dependence on the parameters because of the larger energy gaps in the excited state spectrum. When the decoherence time is small, the damping is so great that states below any of the 3 large gaps in the density of states (see Fig. 3) are essentially cutoff from the coefficient evolution and do not build up sufficient population. The system can only overcome the gaps when the states become very close in energy (a rare event) causing the dynamics to become very slow. On the other hand, the gaps in the spectrum of 2-3-4 PPE are relatively small so that the system is not prevented from hopping even for the smallest values of $\tau_{\beta\alpha}$.

### E. Electronic wavepackets

The width of the electronic wavepackets can be used to demonstrate the effect of the tested decoherence correction on coefficient evolution and on the overall simulated dynamics. We have constructed quantum wavepackets by plotting the square of the coefficient for each state, $|c_\beta|^2$, versus the energy separation from the current state, $\Delta E_{\beta\alpha} = E_\beta - E_\alpha$,

where $\alpha$ denotes the current state. The wavepackets for Standard Tully, ID-S, ID-A, and G-EDC (with recommended parameters) can be seen in Figs. 9 and 10 for PPV3 and 2-3-4 PPE, respectively. For PPV3, the wavepacket evolution is plotted with 2 fs intervals for a total length of 100 fs, and for 2-3-4 PPE the evolution is plotted using 1 fs intervals for a total length of 50 fs. The current state ($\beta = \alpha$) is always located at $\Delta E_{\beta\alpha} = 0$, states below the current state are plotted at negative energy separations, while states at higher energy appear at positive values.

For both systems, Standard Tully propagation results in a broad wavepacket. Lower energy states are immediately populated and gradually grow as they become the new current state. However, most of the population remains in the original higher energy states. The wavepacket of ID-S looks very similar to Standard Tully at short times where a small amount of the population is immediately transferred to the lower energy states. In PPV3, the ID-S wavepacket is much narrower than its Standard Tully counterpart. Yet there is a distinct region where the wavepacket becomes broader as population builds up in higher energy states. This region corresponds to the time between hops when coefficients are evolved according to Standard Tully propagation. Ultimately, the wavepacket becomes narrower again when the coefficients are reset. In contrast, the ID-S wavepacket in 2-3-4 PPE is initially narrow and becomes increasingly wider. The widening to higher energy states occurs after the final effective hop to $S_1$ after which the coefficients are never again reset. In both cases, ID-A narrows the wavepacket and prevents excessive population buildup in the higher energy states by resetting their coefficients to zero once sufficient population has built up there for an attempted hop to occur. Meanwhile population transfer to the lower energy states does not appear to be disrupted. For both systems, G-EDC produces a very narrow wavepacket with respect to the other methods, the population is tightly constrained to the current state even at early times, any broadening is quickly narrowed in the subsequent steps by the rescaling procedure.

Another indication of the coefficient evolution to the lower energy states is to track the ratio of the coefficients of the current state and the state directly below in energy, $\langle |c_{\alpha-1}/c_\alpha| \rangle$, averaged over the swarm of trajectories. The evolution of this coefficient ratio is shown in the top and bottom panels of Fig. 11 for PPV3 and 2-3-4 PPE, respectively, and is compared for the tested decoherence methods. To calculate this quantity, trajectories are removed from the average once they reach the lowest energy $S_1$ state. For both PPV3 and 2-3-4 PPE, the values initially increase, as the quantum wavepacket undergoes broadening from the initial pure state at very early times. In both systems, the ratio is largest for the Standard Tully model and decreases for the various decoherence methods where this decrease corresponds to the decreasing rate of relaxation (see Fig. 6). That is, for large values of $\langle |c_{\alpha-1}/c_\alpha| \rangle$, population buildup in the state directly below the current state is not restricted; in this case, the quantum wavepacket is broad and relaxation is fast. On the other hand, smaller values indicate a narrow wavepacket and slower relaxation dynamics. In general, the ratios are larger for 2-3-4 PPE than for PPV3, reflecting the faster relaxation in the PPE system.
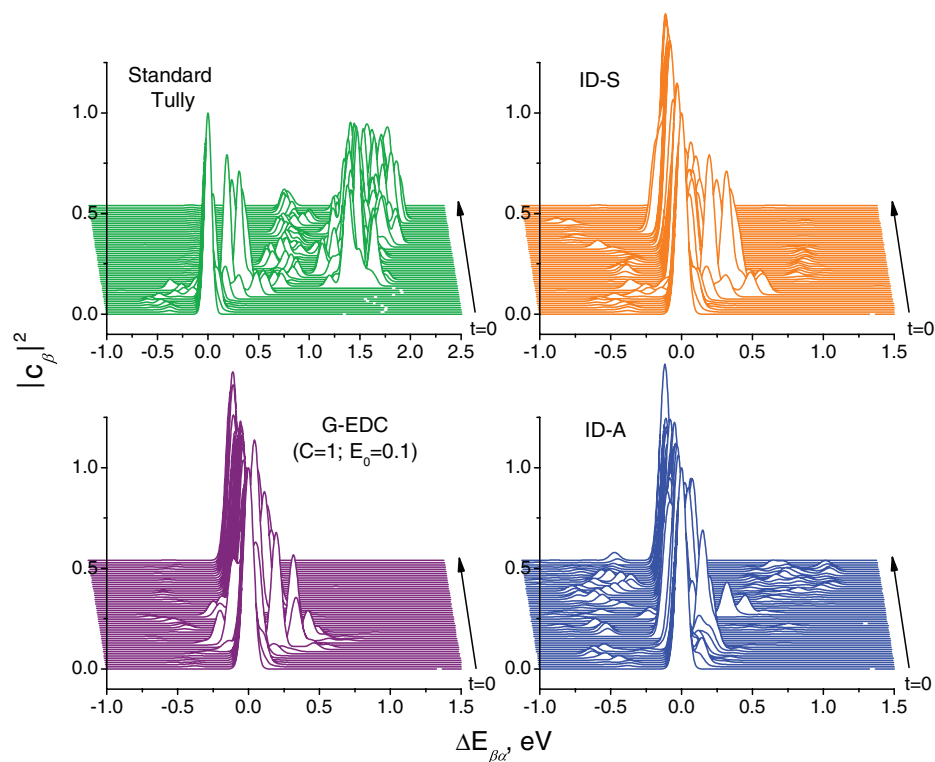
FIG. 9. Quantum wavepacket evolution for relaxation in PPV3 following excitation to $S_m$ compared for the different decoherence methods. The height of each point corresponds to the population of the state with a given energy, where the energy is plotted as the energy difference with respect to the current running state, $\alpha$. Wavepackets are plotted at 2 fs intervals for the first 100 fs of the dynamics.
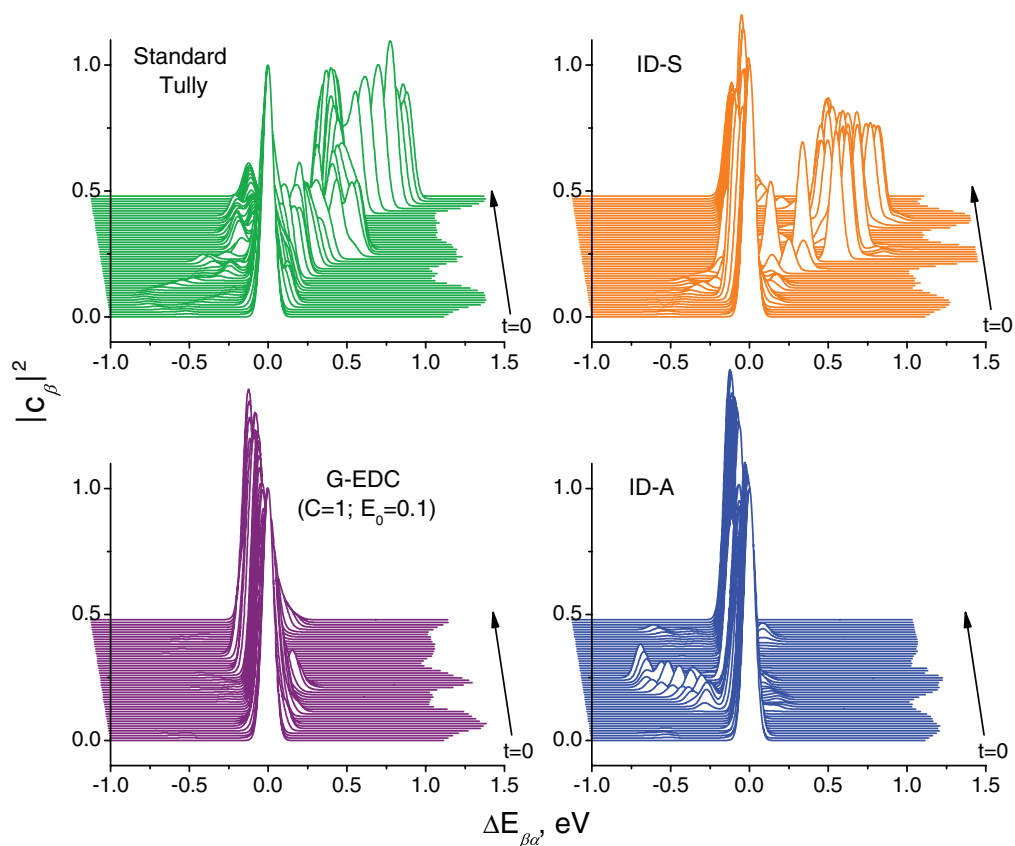


FIG. 10. Quantum wavepacket evolution for relaxation in 2-3-4 PPE following excitation to $S_n$ compared for the different decoherence methods. The height of each point corresponds to the population of the state with a given energy, where the energy is plotted as the energy difference with respect to the current running state, $\alpha$. Wavepackets are plotted at 1 fs intervals for the first 50 fs of the dynamics.
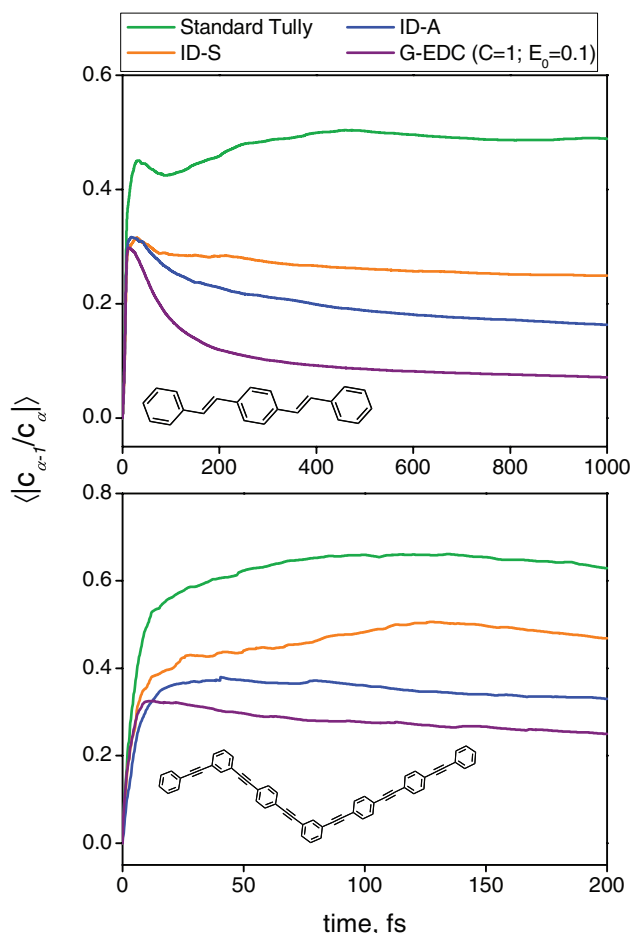
FIG. 11. Time evolution of the ensemble averaged ratio of coefficients for the current state, $\alpha$, and the state directly below in energy, $\alpha - 1$, is compared for the different decoherence methods in (top) PPV3 and (bottom) 2-3-4 PPE.

The ratios are reduced in ID-A compared to ID-S, since the quantity $c_{\alpha-1}$ is reset more often in the case of the former, bringing the ratio to zero (although a nonzero ratio when averaged over the swarm of trajectories). G-EDC produces the lowest ratio where the majority of the population is confined to the current state ($c_\alpha \gg c_{\alpha-1}$). At long times, the G-EDC value saturates to some minimum value ($\langle |c_1/c_2| \rangle$) which is lower in PPV3 than in 2-3-4 PPE because, as we have previously seen, the $S_2$ to $S_1$ energy gap is larger in PPV3 leading to a stronger damping of $c_1$ compared to 2-3-4 PPE.

## IV. CONCLUSIONS

We have demonstrated the importance of incorporating decoherence schemes in MDQT simulations applied to large extended conjugated molecules. Standard Tully surface hopping is an *ad hoc* approach which does not include electronic decoherence. As a result, artifacts appear in simulations as the divergence of the quantum and classical subsystems. Decoherence has a large effect on the accuracy of the simulated dynamics both in terms of time scales for nonradiative relaxation and in promoting internal consistency. We have applied two varieties of instantaneous decoherence procedures (ID-S and ID-A) as well as the energy-based decoherence correction algorithm of Granucci *et al.*[17,18] (G-EDC) to the sim-

ulation of photoinduced dynamics in PPV3 and 2-3-4 PPE at room temperature (300 K). Fifteen excited states were included in the simulation of PPV3, and 10 states were included for 2-3-4 PPE. Compared to the Standard Tully surface hopping algorithm with no decoherence correction, the tested ID and EDC methods restore the internal consistency while at the same time causing the relaxation dynamics to become slower. We have found that, for realistic polyatomic molecules, the simulated results may vary dramatically depending on which decoherence method is used and the corresponding parameters.

At the same time that internal consistency is improved, the overall rate of dynamics becomes slower. This can be understood as a consequence of forcing the electronic coefficients to follow the current state in nuclear propagation. For ID methods, the electronic wavepacket is periodically collapsed to a single electronic state and the quantum coefficients of the divergent wavepackets are erased. Before a hop can occur, a coherent superposition between the two states must be formed. That is, some electronic population must be transferred to states other than the current state. The process of resetting (as in instantaneous decoherence) or rescaling (as in the energy-based algorithms) the quantum amplitudes in order to incorporate decoherence restricts the buildup of electronic population in lower energy states. As a consequence, the transition probabilities are reduced. Ultimately, trajectory hopping becomes less frequent leading to slower dynamics.

All decoherence implementations cause dynamics to slow with respect to the fully coherent Standard Tully propagation, which can be thought of as assigning an infinite decoherence time. At the other end of the spectrum, instantaneous decoherence assumes that divergent wavepackets are immediately decoupled. Standard Tully coherence is maintained in both ID methods before a hop is attempted, and while the coherence is not eliminated in EDC, it is decreased even before any hop is attempted leading to slower transfer. In the case of G-EDC, we found that the recommended parameters (C = 1; $E_0$ = 0.1 hartree) restrict the population buildup in lower energy states by narrowing the quantum wavepacket. We have tested various parameters for the calculation of the decoherence time used in G-EDC and found that the results vary dramatically depending on this choice. For PPV3, large gaps in the density of the excited states produces a strong dependence on the value of $\tau_{\beta\alpha}$. For both of the systems investigated here, the choice of parameters had a large effect on the internal consistency.

In summary, ID provides a simple and low cost method of including decoherence in nonadiabatic molecular dynamics simulations. The results improve internal consistency while at the same time providing a result that does not depend on external parameters and maintains physical relevance. On the other hand, the G-EDC result seems more reliable for systems such as 2-3-4 PPE, with small energy gaps in its spectrum. In this case, the simulated dynamics was relatively stable to changes in parameters, and only the internal consistency was affected. For systems such as PPV3, with multiple large energy gaps, there was no region of stability in the results. In the end, there is no clear recipe for choosing the G-EDC parameters in advance and while the method may be successful

for some systems, it may not work in other cases. The physical relevance of imposing *a posteriori* corrections to include decoherence remains questionable, instead effort should be invested in developing methods in which decoherence effects can be accounted for *a priori*.[45,46] In general, methods that have proven successful for treating small systems do not necessarily translate to larger systems and their success depends on the system under study.

## ACKNOWLEDGMENTS

[1] J. Tully, J. Chem. Phys. **93**, 1061 (1990).
[2] J. C. Tully, J. Chem. Phys. **137**, 22A301 (2012).
[3] T. Nelson, S. Fernandez-Alberti, V. Chernyak, A. E. Roitberg, and S. Tretiak, J. Phys. Chem. B **115**, 5402 (2011).
[4] T. Nelson, S. Fernandez-Alberti, V. Chernyak, A. Roitberg, and S. Tretiak, J. Chem. Phys. **136**, 054108 (2012).
[5] S. Fernandez-Alberti, A. Roitberg, V. Kleiman, T. Nelson, and S. Tretiak, J. Chem. Phys. **137**, 22A526 (2012).
[6] S. Fernandez-Alberti, A. Roitberg, T. Nelson, and S. Tretiak, J. Chem. Phys. **137**, 014512 (2012).
[7] M. Soler, A. Roitberg, T. Nelson, S. Tretiak, and S. Fernandez-Alberti, J. Phys. Chem. A **116**, 9802 (2012).
[8] T. Nelson, S. Fernandez-Alberti, A. E. Roitberg, and S. Tretiak, Phys. Chem. Chem. Phys. **15**, 9245 (2013).
[9] J. Clark, T. Nelson, S. Tretiak, G. Cirmi, and G. Lanzani, Nature Phys. **8**, 225 (2012).
[10] S. Fernandez-Alberti, V. D. Kleiman, S. Tretiak, and A. E. Roitberg, J. Phys. Chem. Lett. **1**, 2699 (2010).
[11] S. Mukamel, *Principles of Nonlinear Optical Spectroscopy* (Oxford, New York, 1995).
[12] E. Neria and A. Nitzan, J. Chem. Phys. **99**, 1109 (1993).
[13] J.-Y. Fang and S. Hammes-Schiffer, J. Phys. Chem. A **103**, 9399 (1999).
[14] J.-Y. Fang and S. Hammes-Schiffer, J. Chem. Phys. **110**, 11166 (1999).
[15] K. Drukker, J. Comput. Phys. **153**, 225 (1999).
[16] E. R. Bittner and P. J. Rossky, J. Chem. Phys. **103**, 8130 (1995).
[17] G. Granucci and M. Persico, J. Chem. Phys. **126**, 134114 (2007).
[18] G. Granucci, M. Persico, and A. Zoccante, J. Chem. Phys. **133**, 134111 (2010).
[19] O. V. Prezhdo and P. J. Rossky, J. Chem. Phys. **107**, 5863 (1997).
[20] B. J. Schwartz, E. R. Bittner, O. V. Prezhdo, and P. J. Rossky, J. Chem. Phys. **104**, 5942 (1996).
[21] J. E. Subotnik and N. Shenvi, J. Chem. Phys. **134**, 024105 (2011).
[22] J. E. Subotnik, J. Phys. Chem. A **115**, 12083 (2011).
[23] N. Shenvi, J. E. Subotnik, and W. Yang, J. Chem. Phys. **134**, 144102 (2011).
[24] C. Zhu, S. Nangia, A. W. Jasper, and D. G. Truhlar, J. Chem. Phys. **121**, 7658 (2004).
[25] M. Thachuk, M. Y. Ivanov, and D. M. Wardlaw, J. Chem. Phys. **109**, 5747 (1998).
[26] F. Webster, P. J. Rossky, and R. A. Friesner, Comput. Phys. Commun. **63**, 494 (1991).
[27] B. F. Habenicht and O. V. Prezhdo, Phys. Rev. Lett. **100**, 197402 (2008).
[28] B. F. Habenicht and O. V. Prezhdo, J. Phys. Chem. C **113**, 14067 (2009).
[29] M. Barbatti and H. Lischka, J. Am. Chem. Soc. **130**, 6831 (2008).
[30] M. Barbatti *et al.*, J. Chem. Phys. **137**, 22A503 (2012).
[31] F. Plasser *et al.*, J. Chem. Phys. **137**, 22A514 (2012).
[32] M. D. Hack and D. G. Truhlar, J. Chem. Phys. **114**, 9305 (2001).
[33] S. Hammes-Schiffer and J. C. Tully, J. Chem. Phys. **101**, 4657 (1994).
[34] S. Tretiak and S. Mukamel, Chem. Rev. **102**, 3171 (2002).
[35] S. Mukamel, S. Tretiak, T. Wagersreiter, and V. Chernyak, Science **277**, 781 (1997).
[36] S. Tretiak, V. Chernyak, and S. Mukamel, J. Chem. Phys. **105**, 8914 (1996).
[37] S. Tretiak, W. M. Zhang, V. Chernyak, and S. Mukamel, Proc. Natl. Acad. Sci. U.S.A. **96**, 13003 (1999).
[38] V. Chernyak, M. F. Schulz, S. Mukamel, S. Tretiak, and E. V. Tsiper, J. Chem. Phys. **113**, 36 (2000).
[39] S. Tretiak, A. Saxena, R. L. Martin, and A. R. Bishop, Phys. Rev. Lett. **89**, 097402 (2002).
[40] E. Fabiano, T. W. Keal, and W. Thiel, Chem. Phys. **349**, 334 (2008).
[41] M. Paterlini and D. Ferguson, Chem. Phys. **236**, 243 (1998).
[42] H. Zhao, S. Mazumdar, C. X. Sheng, M. Tong, and Z. V. Vardeny, Phys. Rev. B **73**, 75403 (2006).
[43] S. V. Frolov, Z. Bao, M. Wohlgenannt, and Z. V. Vardeny, Phys. Rev. Lett. **85**, 2196 (2000).
[44] E. R. Bittner and P. J. Rossky, J. Chem. Phys. **107**, 8611 (1997).
[45] H. M. Jaeger, S. Fischer, and O. V. Prezhdo, J. Chem. Phys. **137**, 22A545 (2012).
[46] V. N. Gorshkov, S. Tretiak, and D. Mozyrsky, "Semiclassical Monte-Carlo approach for modeling non-adiabatic dynamics in extended molecules," Nature Comm. (in press).